Self-Assembly of Rod−Coil Block Copolymers and Their Application in Electroluminescent Devices

Yuefei Tao,[†,§] Biwu Ma,[†,§] and Rachel A. Segalman*[,‡,§]

Department of Chemistry and Department of Chemical Engineering, University of California, Berkeley, California 94720, and Materials Science Division, Lawrence Berkeley Laboratory, Berkeley, California 94720

Received March 14, 2008; Revised Manuscript Received July 14, 2008

ABSTRACT: The formation of alternating electron transporting and hole transporting 15 nm lamellae within the active layer of an organic light-emitting diode (OLED) is demonstrated to improve device performance. A new multifunctional bipolar rod−coil block copolymer containing a poly(alkoxy phenylenevinylene) (PPV) rod-shaped block as the hole transporting and emitting material and a poly(vinyloxadiazole) coil-shaped electron transporting block is synthesized. This new block copolymer is the active material of a self-assembling multicomponent electroluminescent device that can be deposited in a single step. In the thin film, grazing incidence X-ray scattering and transmission electron microscopy demonstrate that the layers form grains which are oriented bimodally: parallel and perpendicular from the anode. In this mixed orientation, the device demonstrates better performance than those with either pure PPV or a blend of the two analogous homopolymers as the active materials, i.e., higher external quantum efficiency (EQE) and brightness. This improved device performance is mainly attributed to the bipolar functionality and microphase separation of the block copolymer, which provide highly efficient hole and electron recombination at the nanodomain interfaces.

Introduction

Organic light-emitting diodes are attractive for display technologies due to their inherently low materials costs, excellent stabilities, high efficiencies, broad color tunabilities, and the possibility of scalable processing and production.[1−4] Optimal device performance depends crucially on balanced charge injection and transport through the device, a requirement that has best been satisfied by the incorporation of at least two materials optimized for electron and hole transport.[5] Maximal interfacial area between electron and hole transporting materials is also necessary to facilitate the exciton formation.[1] Multilayer structures incorporating hole transporting layers, emitting layers, and electron transporting layers sandwiched between the two electrodes have been fabricated by the high-vacuum sublimation and vapor deposition of small molecule components (Scheme 1a). These intricate devices generally exhibit superior device performance.[6−10] Polymeric materials may be more easily and inexpensively solution processed, but it is difficult to process multilayer structures. One approach to overcoming these processing challenges uses cross-linking technologies that will allow sequential layer deposition via sequential solution processing steps.[11−14] Alternately, single step processing may be achievable through the use of polymer blends[15−19] and random or block copolymers.[20−27]

Block copolymers have both the chemical advantage of sequestering the different electronic functionality to the ends of the chain and the promise of self-assembling nanostructures with a very high degree of regularity at the 10 nm length scale.[28] While the spherical, cylindrical, bicontinuous, and lamellar nanostructures of classical block copolymers are very alluring for organic electronic applications, the conjugated backbone of most light-emitting polymers rigidifies the chain and fundamentally alters the thermodynamics of self-assembly. The self-assembly of rod−coil systems is controlled not only by the interactions between blocks but also by the liquid crystalline behavior of the rod block. Predictions indicate that the interplay between microphase separation and liquid crystallinity creates thermodynamics and equilibrium microphase structures that are distinct from classical coil−coil block copolymer systems.[29−36] Solution and thermally self-assembled polymeric materials have demonstrated a number of intriguing phases including wavy lamellae,[37] zig-zags,[37] arrowheads,[37] straight lamellae,[38,39] perforated lamellae,[39−41] hexagonal strips,[38,42,43] pucks,[39,42−44] and spheres.[45,46] Shorter chains which appear to be strongly stretched exhibit even more phases including cylindrical[47−49] and bicontinuous cubic[38,50,51] morphologies. The subject of rod−coil self-assembly is an active area of research and the subject of several reviews.[52−57] We recently demonstrated a phase diagram of a model conjugated poly(alkoxy phenylenevinylene) rod−coil block copolymer with thermally accessible order−disorder transitions, which agrees well with several predictions.[58−60] This model rod−coil block copolymer system self-assembles into only lamellar and hexagonally symmetric structures with changing coil volume fraction and temperature. Liquid crystalline interactions appear to stabilize the planar interfaces such that they occupy a larger portion of phase space than in classical block copolymers,[58] though Sary et al. have recently observed the formation of spheres in a related system.[45,46]

Most organic electronics and other applications rely on the thin film architecture of rod−coil block copolymers. Because of incommensurability between the average film thickness and the natural domain spacing of block copolymer lamellae oriented parallel to a substrate, islands and holes form in submonolayer films of rod−coil oligomers and polymers.[61−64] Pereira and Williams performed calculations for rod−coil molecules confined between two hard interfaces and found that when the film thickness is incommensurate with the block copolymer domain spacing, incommensurability is accommodated through changes in the rod tilt angle relative to the lamellar normal as well as reorientation of lamellar domains to be perpendicular to the substrate.[65] Thin films of conjugated rod−coil block copolymers have been shown to self-assemble into a lamellar microphases upon thermal annealing with the lamellae oriented primarily parallel to the substrate. Grains of lamellae with parallel orientation are characterized by irregular polygon shapes and

* Corresponding author: e-mail segalman@berkeley.edu.
† Department of Chemistry, University of California Berkeley.
‡ Department of Chemical Engineering, University of California Berkeley.
§ Lawrence Berkeley Laboratory.

10.1021/ma800577g CCC: $40.75 © 2008 American Chemical Society
Published on Web 09/17/2008

Scheme 1. (a) Typical High-Efficiency OLEDS Contain Many Layers Made from Small Molecule Components Sequentially Evaporated onto the Anode; (b) Self-Assembly at the 10 nm Length Scale Could Be Used To Incorporate Similar Features into a Device Which May Be Solution Processed in a Single Step

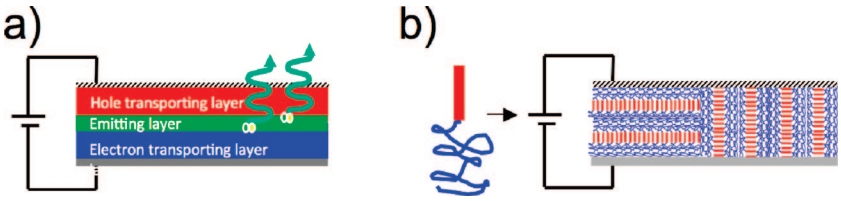

Scheme 2. Chemical Structure of a Bipolar Rod−Coil Block Copolymer

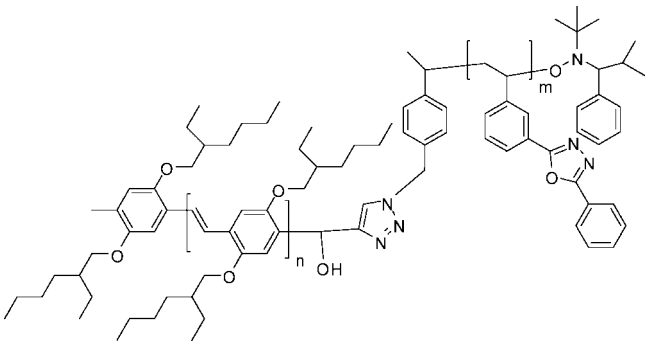

are bounded by defect regions where the lamellae are oriented perpendicularly out of the plane of the film, resulting in an unusual bimodal orientation of lamellae both parallel and perpendicular to the substrate.[66,67]

For organic electronic applications, the block copolymer should contain both electron-donating and -accepting blocks for photovoltaics or electron transporting, hole transporting, and even emitting and blocking layers in OLEDs. The domain size of self-assembled rod−coil block copolymers can be controlled through molecular weight on the scale of 5−100 nm, which overlaps well with the ∼10 nm length scale of exciton diffusion.[5,68−70] Several groups have prepared block copolymer systems containing both p- and n-type functional blocks for OLEDs[24−27,71−74] and photovoltaics,[75−79] with only a few demonstrating the long-range order typical of block copolymer self-assemblies.[80−85] Prior studies on nonconjugated bipolar block copolymers indicate that the nanophase segregation of components (as opposed to the mixing inherent in random copolymers) is advantageous to OLED performance.[27] It is advantageous to gain similar nanophase segregation in block copolymers containing more commonly used light-emitting polymers with extended chain conjugation. This presents two major hurdles: synthetic and self-assembly. Well-defined nanostructures result from well-defined (both molecular weight and polydispersity control) block copolymers. Most conjugated polymers are made via condensation routes and are highly polydisperse, though a few routes exist toward molecular weight and polydispersity control.[86−89] In addition, conjugated polymers, as previously discussed, tend to have rigid backbones, and their self-assembly is not the same as classical block copolymer systems.

In this paper, the synthesis of a bipolar rod−coil block copolymer (as shown in Scheme 2) incorporating a standard emission block (poly(alkoxy phenylenevinylene)) (PPV) and an electron transporting moiety (oxadiazole) tethered to a coil-like backbone is demonstrated. The block copolymer is demonstrated to form lamellar layers with a spacing of 15.1 nm with the lamellar interface distributed both parallel to and perpendicular from the electrodes, as sketched in Scheme 1b. Self-assembled thin film devices outperform pure poly(alkoxyphenylenevinylene) and blends made from analogous homopolymers of poly(vinyloxadiazole) and poly(alkoxyphenylenevinylene). The higher external quantum efficiency (EQE) and brightness of the nanostructured device clearly demonstrate the importance of nanostructural control for device optimization.

Experimental Methods

Materials. All reactions were run under N_2 unless otherwise noted. NMR spectra were recorded on Bruker DRX-500 or AVX 400 instrument. Analytical SEC in THF was performed at 35 °C at a nominal flow rate of 1.0 mL/min on a chromatography line fit with three columns having pore sizes of 105, 103, and 500 Å, calibrated with monodisperse polystyrene standards (162−2 100 000 Da). Precursors 2-(3-ethenylphenyl)-5-phenyl-1,3,4-oxadiazole[25] and the alkoxyamine initiator[90] were synthesized according to references. All other reagents were obtained from Aldrich and used as received.

Synthesis of Alkyne-Functionalized Poly(2,5-di(2′-ethylhexyloxy)-1,4-phenylenevinylene), 1. Narrow polydispersity PPV was synthesized by Seigrist polycondensation, as previously described.[58] To achieve alkyne end functionality, 1 mL of a 0.5 M solution of ethynylmagnesium bromide in THF was added to PPV (1 g, 0.28 mmol) solution in 50 mL of dry THF under nitrogen for 10 min. After reaction, the polymer was precipitated in methanol, yielding an orange polymer (0.95 g, 95%). ^{1}H NMR ($CDCl_3$) δ: 0.89 (m, 12(n + 1)H, −C*H*3), 1.45 (m, 16(n + 1)H, −C*H*2−), 1.81 (m, 2(n + 1)H, −C*H*−), 2.24 (s, 3H, Ar−C*H*3), 2.64 (t, 1H, *H*O−), 3.14 (d, 1H, *H*−C≡C), 3.96 (m, 4(n + 1)H, −O−C*H*2−), 5.68 (d, 1H, Ar−C*H*−C≡C), 7.20 (s, 2nH, −C*H*d), 7.53 (s, 2(n + 1)H, Ar−*H*).

Synthesis of Chloride End-Functionalized Poly(2-(3-ethenylphenyl)-5-phenyl-1,3,4-oxadiazole), 2. A mixture of alkoxyamine (121 mg, 0.32 mmol) and 2-(3-ethenylphenyl)-5-phenyl-1,3,4-oxadiazole (2.5 g, 10 mmol) was degassed by three freeze−pump−thaw cycles, sealed under vacuum, and heated at 125 °C for 3 h. The viscous reaction mixture was then dissolved in THF and precipitated twice in methanol to give **2** as a white powder (1.5 g, 60%, M_n = 5800 g/mol, PDI = 1.20). ^{1}H NMR ($CDCl_3$) δ: 0.42−1.90 (m, aliphatic H), 4.35 (m, CH_2−Cl), 6.53−7.82 (m, aromatic H).

Synthesis of Azide End-Functionalized Poly(2-(3-ethenylphenyl)-5-phenyl-1,3,4-oxadiazole), 3. Polymer **2** (1.5 g, 0.32 mmol) was dissolved in DMF (10 mL), and sodium azide (208 mg, 3.2 mmol) was added. The reaction mixture was stirred for 22 h at 60 °C. After reaction, the polymer was precipitated in methanol, yielding a white powder (1.45 g, 96%). ^{1}H NMR ($CDCl_3$) δ: 0.42−1.90 (m, aliphatic H), 4.53 (m, CH_2−N_3), 6.53−7.82 (m, aromatic H).

Synthesis of Poly(2,5-di(2′-ethylhexyloxy)-1,4-phenylenevinylene)-*block*-(2-(3-ethenylphenyl)-5-phenyl-1,3,4-oxadiazole), 4 (PPV-*b*-OX). Alkyne end-functionalized PPV **1** (0.71 g, 0.2 mmol), azide end-functionalized POX **2** (1.07 g, 0.23 mmol), and CuI (7.8 mg, 0.04 mmol) were placed in a Schlenk tube which was evacuated and back-filled with dry nitrogen. The procedure was repeated three times. After the evacuating cycles, THF (20 mL) and 1,8-diaza[5.4.0]bicycloundec-7-ene (500 mg, 3.3 mmol) were added, and the reaction mixture was placed in a statically controlled oil bath at 35 °C for 18 h. After reaction, the polymer was dissolved in dichloromethane and washed with a 0.065 M EDTA solution.

Scheme 3. Synthesis Route of the PPV-*b*-OX Block Copolymers

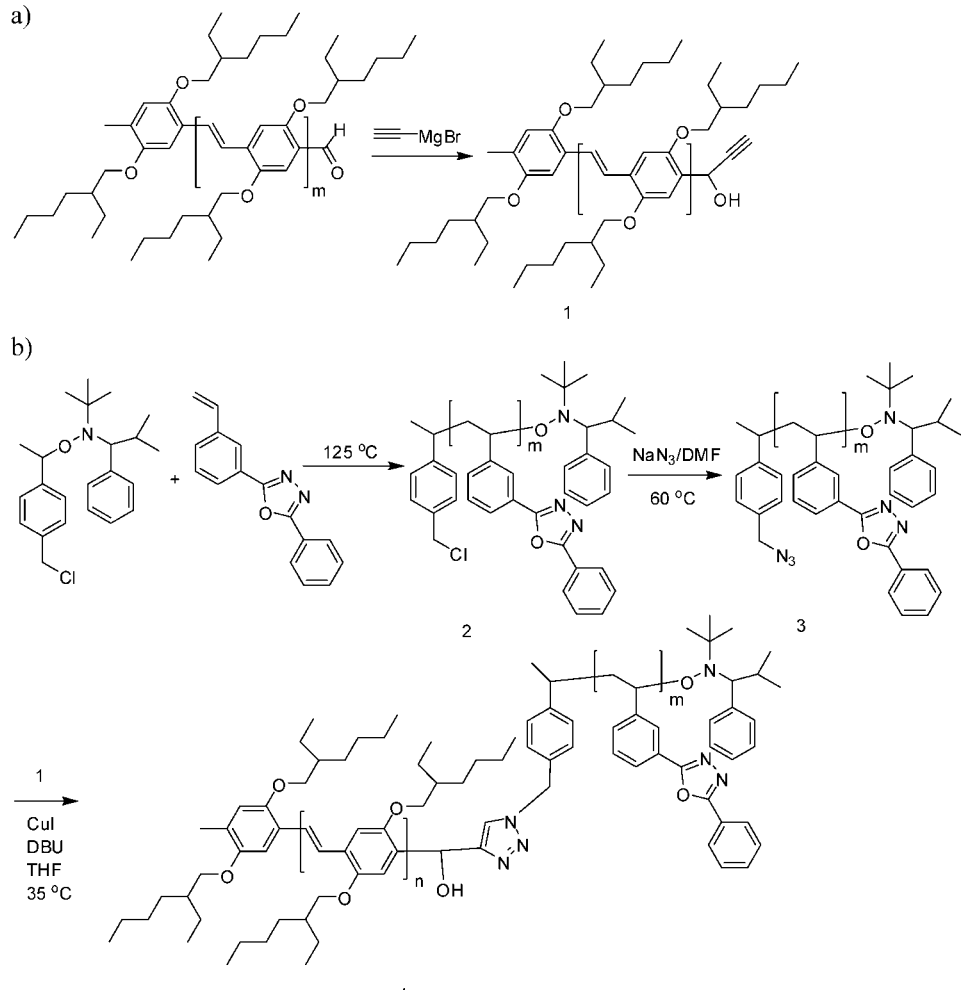

The organic layer was dried with anhydrous magnesium sulfate and was concentrated in vacuo. The polymer was fractionated,

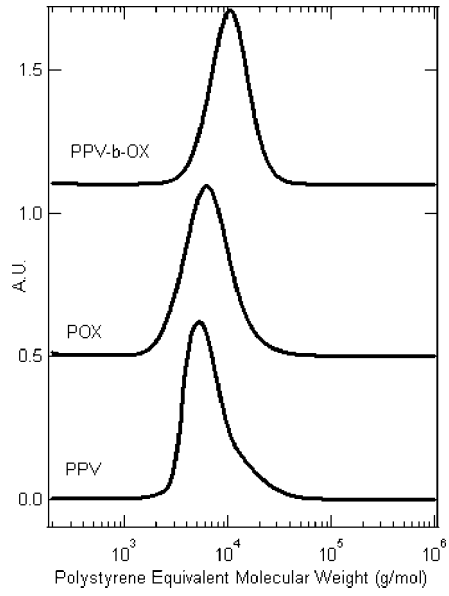

Figure 1. GPC of block copolymer PPV-*b*-OX and its precursors (analogous homopolymers, PPV and POX). The PPV-*b*-OX was synthesized by the "click reaction" of PPV and POX. The increased molecular weight and low polydispersity of the block copolymer indicates the success of the coupling reaction.

Table 1. PPV, POX, and Block Copolymer PPV-*b*-OX

polymer	M_n (g/mol) (GPC)	M_n (g/mol) (NMR)	M_w/M_n (GPC)
PPV	4500	3500	1.17
POX	5800	4500	1.20
PPV-*b*-OX	10500	8000	1.20

yielding an orange solid (1.5 g, 90%, M_n = 10 500 g/mol, PDI = 1.20). ^{1}H NMR ($CDCl_3$) δ: 0.42−1.90 (m, aliphatic H), 2.24 (s, Ar−C*H*3), 3.96 (m, −O−C*H*2−), 6.53−7.82 (m, aromatic H).

General Characterization Methods. Small-angle X-ray scattering (SAXS) experiments were performed on beamline 1-4 of the Stanford Synchrotron Radiation Laboratory (SSRL). The beamline was configured with an X-ray wavelength of 1.488 Å and focused to a spot size of ~0.5 mm diameter. Samples for SAXS was prepared by annealing polymers at 180 °C in vacuum for 22 h to form 1 mm thick disks and then sealing the sample between Kapton windows.

Transmission Electron Microscopy. TEM was performed to observe the real-space bulk morphology of the rod−coil block copolymer. Samples were prepared for transmission electron microscopy (TEM) were prepared by first spin-casting films from chloroform solutions (10 mg/mL) onto NaCl freshly cleaved from a single crystalline ingot. Film thickness was controlled by concentration and spin speed to be 80 nm. Block copolymer layer thicknesses were measured on dummy samples spun-coat under identical condition directly onto Si wafers using a Rudolph Technologies AutoEL ellipsometer. The samples were then annealed under high vacuum (10^{-6} Torr) at 180 °C for 22 h and then cooled slowly to room temperature. The polymer films were then floated off of the NaCl substrate and onto a water bath where they were retrieved ontop of a 500 mesh copper TEM grid. To create TEM

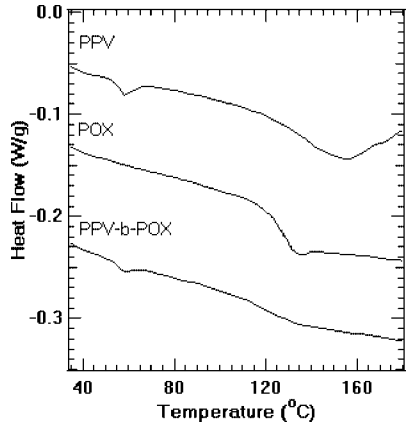

Figure 2. Differential scanning calorimetry (DSC) of PPV, POX, and PPV-*b*-POX at heating rates of 10 °C/min. The block copolymer demonstrates both the melting transition of the PPV block and the higher temperature transition observed in POX.

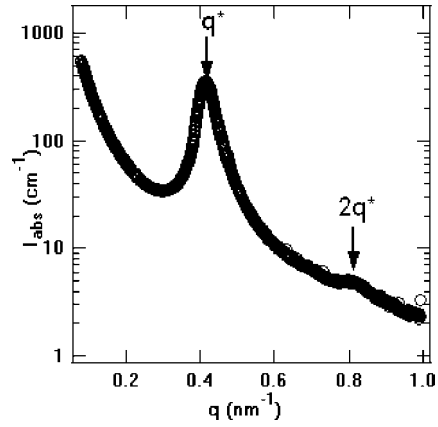

Figure 3. SAXS of bipolar block copolymer at 30 °C. The block copolymer is self-assembles into lamellae with spacing of 15.1 nm, as indicated by peaks at integer multiples of its respective q^*.

contrast, the poly(vinyloxadiazole) domains were preferentially stained by exposure to the vapor from a 2% OsO_4 solution for 4 h. TEM images were obtained on a FEI Tecnai 12 (100 kV, bright field) using the internal charge-coupled device (CCD) camera. Sample preparations similar to the device structure (with a poly(styrenesulfonate)-doped poly(3,4-ethylenedioxythiophene) (PEDOT:PSS) substrate layer) were not possible due to strong adhesion between the polymer layers after annealing. Since the TEM substrate conditions do not match those of the devices, lamellar orientation in these images do not necessarily match devices. Further experiments discussed below provide details on lamellar orientation.

GISAXS Experiment. The orientation of lamellae relative to the electrodes in device architectures was observed via grazing-incidence small-angle X-ray scattering (GISAXS). To mimic the device architecture, a PEDOT:PSS-coated (100) silicon wafer was used as the substrate, onto which the block copolymer was spun-cast from chloroform. Eighty nanometer film thicknesses were achieved from 10 mg/mL solutions and 1000 rpm spin speeds. Block copolymer layer thicknesses were measured on dummy samples spun-coat under identical condition directly onto Si wafers as previously discussed. Samples were annealed under high vacuum at 180 °C for 22 h and then cooled slowly to room temperature.

GISAXS experiments were performed at beamline 8-ID-E of the Advanced Photon Source using an experimental geometry similar to that described previously.[91,92] Experiments were performed using a 1.664 Å X-ray beam with a width of 100 μm and a height of 50 μm. Data were recorded on a 2D CCD detector, and the sample to detector distance was 2.27 m. Data were acquired for 30 s per frame at an incident angle of 0.175° (above the critical such that the X-ray penetration depth was much larger than the film thickness), and three frames from different spots on the sample were added to generate the scattering plot. Scattering angles were converted into q-space accounting for the planarity of the detector. The q_z axis is calculated using the direct beam as the reference beam and holding q_{xy} fixed at zero. The q_{xy} axis is similarly calculated, holding q_z fixed at zero. Although the geometry of the grazing incidence experiment creates distortions in q-space (such that the domain spacing is not equal to $2\pi/q^*$), the q_z and q_{xy} axes approximate a Cartesian coordinate system to a high degree of accuracy in the small-angle regime and are plotted in this manner. Scattering intensities are reported in arbitrary units.

Device Fabrication and Characterization. Prepatterned ITO (150 ± 7.5 nm thickness) on glass substrates with 2 mm wide stripes and resistivities of 20 Ω/sq were cleaned as described previously.[27] A 40 nm thick PEDOT:PSS layer was spun-coat at a rate of 4000 rpm onto the ITO. The organic active layers were then prepared by spin-coating the block copolymer from filtered chloroform solutions at 1000 rpm, varying the concentration to achieve 80 nm thick films. Two millimeter wide, 1 nm thick LiF covered with 100 nm thick aluminum cathodes were deposited through a shadow mask at rates of 0.2 (LiF) and 4−5 (Al) Å/s in a vacuum chamber with base pressure below 3×10^{-6} Torr. The devices were tested in air within 2 h of fabrication. The electrical and optical intensity characteristics of the devices were measured with a Keithly 2400 sourcemeter/2000 multimeter coupled to a Newport 1835-C optical meter, equipped with a UV-818 Si photodetector. Only light emitting from the front face of the device was collected and used in subsequent efficiency calculations. The electroluminescence (EL) spectra were measured on a USB4000 miniature fiber-optic spectrometer. The emission was found to be uniform throughout the area of each device.

Results and Discussion

Synthesis and Characterization of Block Copolymers. Monodisperse homopolymers of rodlike PPV and coil-shaped poly(vinyloxadiazole) were synthesized and then coupled via 1,3-dipolar cycloaddition reactions between the azide and alkyne end groups using CuI and 1,8-diaza [5.4.0]bicyloundec-7-ene (DBU)[93] to form block copolymers. Narrow polydispersity aldehyde end-functionalized alkoxy-PPV ($M_n = 3.5$K, PDI = 1.17) was prepared through a Seigrist polycondensation as previously reported.[58] An alkyne end-functionality was then attached (**2**) through the nucleophilic attack of a Grignard reagent on the aldehyde group (Scheme 3a). An excess of the Grignard reagent guaranteed complete functionalization, as evidenced by the disappearance of the aldehyde signal in ^{1}H NMR (not shown). The solubility of the Grignard reagent facilitates subsequent purification of the resulting alkyne end-functionalized PPV. The number-average molecular weight was determined to be 3500 g/mol with a polydispersity index of 1.17, as determined from a combination of ^{1}H NMR and size exclusion chromatography (SEC) using polystyrene standards, shown in Figure 1.

Azide end-functionalized poly(vinyloxadiazole) (POX) (**3**) was prepared via a nitroxide-mediated living free radical polymerization route using a chloride-functionalized alkoxyamine as the initiator as shown in Scheme 3b. As shown by GPC in Figure 1, the polymerization was well controlled and resulted in narrow polydispersities of ~1.2. A single azide end group on the polymer chain was created by substituting the chloride introduced in the initiator with sodium azide. The chloride group was converted into azide (conversion >90%) according to ^{1}H NMR, as depicted in Scheme 3b.

The block copolymers (**4**) were formed via "click reactions" between the azide-end-functionalized POX (**3**) and the alkyne-functionalized PPV (**1**) using CuI and 1,8-diaza [5.4.0]bicycloundec-7-ene (DBU)[93] catalysts (Scheme 3b). The click reactions were performed in an excess of PPV, and the products

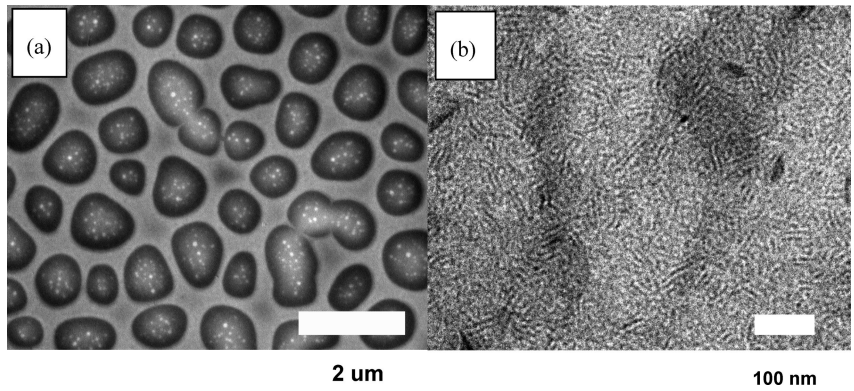

Figure 4. Transmission electron micrographs of PPV/POX blend and PPV-*b*-OX block copolymer cast and annealed on NaCl crystals to demonstrate degree of order. Samples are stained with OsO_4 which makes the POX rich domains appear dark. (a) The PPV/POX blend (1:1 weight ratio) shows macrophase separation at the micron length scale. (b) PPV-*b*-OX with annealing at 180 °C for 22 h forms a defective lamellar structure with the planes oriented perpendicular to the plane of view. Note: the substrate conditions necessary for TEM do not match device substrates.

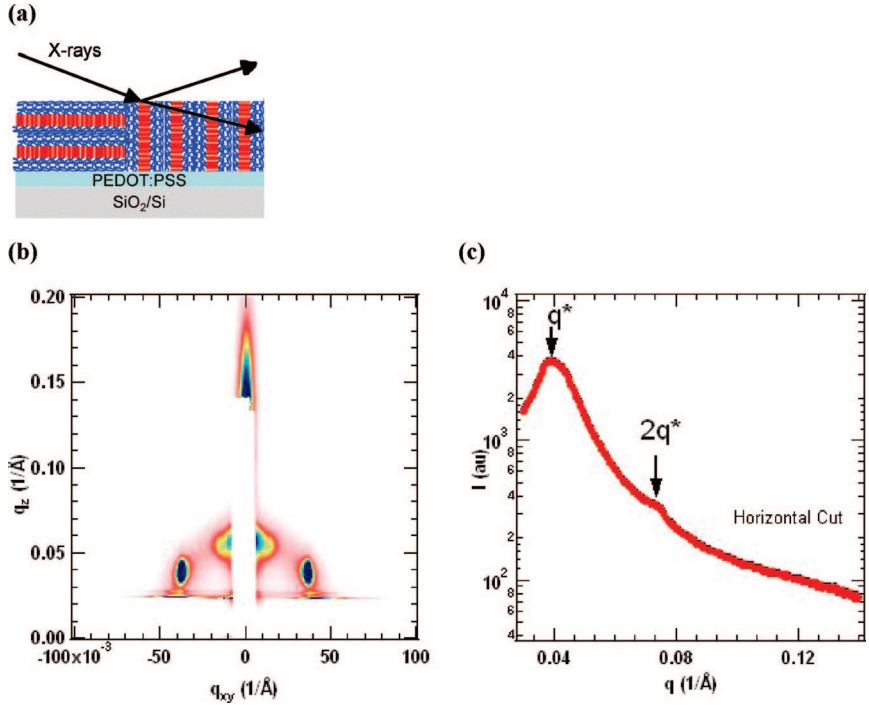

Figure 5. Lamellar structure in thin films on PEDOT:PSS substrates. (a) Sample geometry for GISAXS experiment is similar to the device geometry (PEDOT:PSS substrate). (b) A GISAXS scattering pattern taken above the critical angle for PPV-*b*-POX integrates over the depth of the film. Scattering peaks only in the q_z and q_{xy} directions indicate lamellae oriented bimodally out of and in the plane of the substrate. The film thickness is 80 nm, and the X-ray incident angle is 0.175°. (c) Line cut taken from the two-dimensional image illustrates higher order peaks consistent with the lamellar structure. Full distorted Born wave approximation analysis indicates that domain spacings in both the parallel and perpendicular directions are 15.8 nm.

were fractionated from THF and methanol. After fractionation, no residual starting material was observed, and SEC traces of the block copolymers (Figure 1) demonstrate the expected shifts toward higher molecular weights indicative of block copolymer formation. Moreover, no increase of the PDI was observed upon block copolymer formation, which implies that the coupling reactions went to completion. Table 1 summarizes the characteristics of the two homopolymers (PPV and POX) and the PPV-*b*-OX block copolymer.

Self-Assembly of the Block Copolymer. The nanostructure of the active layer plays a crucial role in controlling the device performance, and therefore careful study was done of the nanometer scale morphology. Here, small-angle X-ray scattering in transmission mode is used to probe the bulk morphology (mm thick samples) and in grazing incidence mode to probe the thin film structure (samples less than 100 nm thick on substrates matching the device geometry).

Differential scanning calorimetry (DSC) of the PPV homopolymer indicates a melting transition 58 °C, similar to that previously documented.[94] The block copolymer exhibits both this transition and the higher glass transition temperature (130 °C) of the POX block, as shown in Figure 2. Above 130 °C, the block copolymer is mobile and able to self-assemble. It decomposes at temperatures above ~300 °C when annealed under high vacuum (10^{-6} Torr). Bulk samples of PPV-*b*-OX block copolymer were annealed under high vacuum at 180 °C for 22 h and then cooled slowly to room temperature to achieve self-assembly.

These annealed samples demonstrate small-angle X-ray scattering (SAXS) peaks at integer spacings, indicative of a lamellar nanostructure with a spacing of 15.1 nm, as shown in Figure 3. The second order peak ($2q^*$) is disallowed by the form factor in symmetric lamellae, and its diminished character is common in systems of nearly symmetric lamellae.[95] Real-space

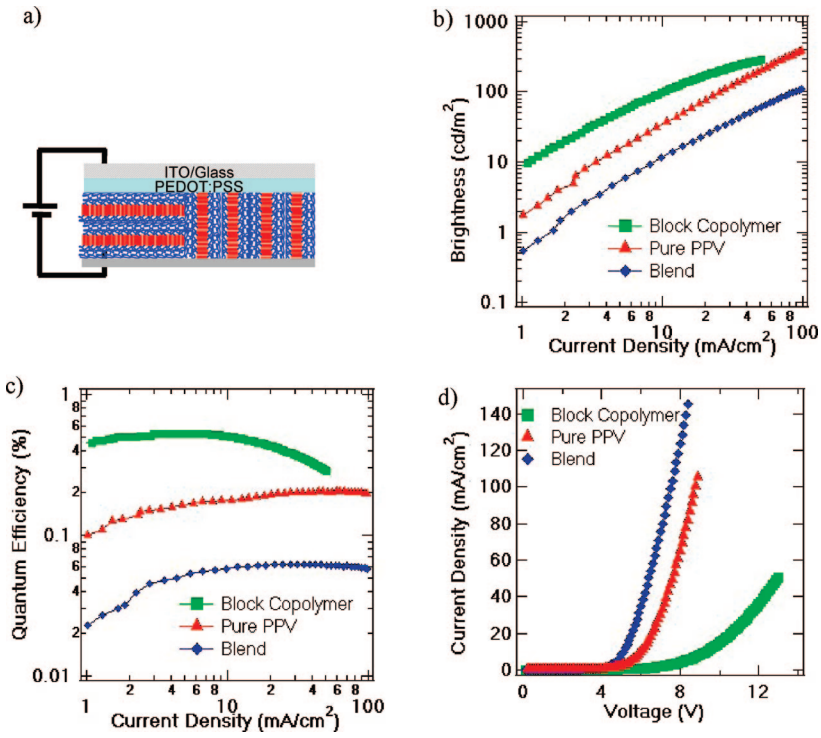

Figure 6. Block copolymer OLED's are spun-coat on glass/ITO/PEDOT:PSS and then capped with LiF/Al electrodes (a). The block copolymer demonstrates superior external quantum efficiency (b), brightness as a function of current density (c), and $I-V$ characteristics (d) than comparable pure homopolymer PPV and PPV/POX blends.

imaging via TEM was performed to confirm the lamellar nanostructure, with contrast enhancement achieved by preferentially staining poly(vinyloxadiazole) with OsO_4. Preferential staining was confirmed by staining of blends of varying compositional ratios. As shown in Figure 4a, the blend components macrophase separated into micrometer-scale features clearly visible as PPV-rich (light) and POX-rich (dark) regions. The annealed block copolymer shows nanoscale phase separation (Figure 4b) with well-controlled width (~15 nm) characteristic of lamellae with good microphase separation but poor long-range order.[96]

Substrate conditions largely control block copolymer lamellar orientation, so great care was taken to observe lamellar orientation and long-range order in device-similar thin film geometries via grazing incidence X-ray scattering (GISAXS). In order to mimic the real device structure, the block copolymer was spun-cast onto a PEDOT:PSS coated silicon wafer as shown in Figure 5a. When the angle of X-ray incidence is above the critical angle of the polymer, the X-rays fully penetrate the film and the resulting scattering pattern (as shown in Figure 5b) samples structures throughout the entire film thickness. This scattering pattern shows peaks only along the q_z and q_{xy} axes. Peaks along q_z originate from lamellae oriented parallel to the film, while peaks along q_{xy} are from perpendicularly oriented lamellae,[67] indicating that lamellae form along only these two orthogonal directions, as schematically shown in the inset of Figure 5. Line cuts through the two-dimensional GISAXS image show higher order peaks consistent with lamellar structure in both the parallel and perpendicular directions. GISAXS is a semikinematic scattering technique in which both the incoming and outgoing waves are distorted by the film. As a result, the domain spacing is not simply given by $2\pi/q^*$. Upon calculation within the distorted wave Born approximation (DWBA),[91,92,97] the domain spacings in both the parallel and perpendicular directions from the substrate were calculated to be ~15.8 nm, similar to the bulk value. Although classical block copolymer lamellae tend to orient unidirectionally parallel or perpendicular to the substrate,[98] previous studies indicate that PPV containing rod−coil block copolymer lamellae tend bimodally both parallel and perpendicular to the substrate due to a combination of kinetic trapping and differences in defect energies.[66,67]

Electroluminescent Devices. Here, we use the self-assembled lamellar structures of rod−coil block copolymers to mimic the multicomponent structure common to OLEDs without the costly multistep fabrication techniques. Highly efficient organic light-emitting diodes typically contain at least three layers: a hole transporting layer, an emitting layer, and an electron transporting layer sequentially evaporated onto an ITO anode, as shown in Scheme 1a. Electron and hole transporting layers help balance charge injection and transport. Electrons and holes recombine to form excitons in the emitting layer which is often chosen to tune emission wavelength or to allow for better light emission[7,8] The brightness and efficiencies from a PPV-*b*-OX, a blend of analogous homopolymers, and a pure PPV control are compared to demonstrate the effect of nanostructure on device performance.

As previously discussed, the PPV-*b*-OX block copolymer self-assembles into lamellae with an ~15 nm spacing with grains both parallel and perpendicular from the interface. Since PPV is a good hole transporting and emitting material and oxadiazole is a good electron transporting material, self-assembled PPV-*b*-OX is a good model system to test the effects of nanostructure. To evaluate how the self-assembled structure effects device performance, single-layer light-emitting devices with the configuration of ITO/PEDOT:PSS/polymer/LiF/Al (Figure 6a) have been fabricated and investigated. The self-assembled device shows better external quantum efficiency and brightness than the pure PPV device at the same current density (Figure 6b,c). For example, at 10 mA/cm^2, self-assembled device shows 0.5% EQE and 103 cd/m^2 brightness which are 2.7 times higher than pure PPV device. We speculate that the nanostructured lamellae in the block copolymer device have a maximum effective interfacial area between the electron and hole transporting

domains, which facilitates the formation of excitons even if the lamellae are not unidirectionally oriented with respect to the electrodes.

Prior studies indicate that blending electron transporting materials with hole transporting materials produces efficient devices,[16] so the self-assembled device is compared to one composed of an analagous blend of homopolymer POX (electron transporting material) and PPV (hole transporting material). The blend device demonstrates inferior external quantum efficiency and brightness when compared to either the pure PPV device or the block copolymer device at the same current density (Figure 6b,c). For example, at 10 mA/cm^2, the blend device demonstrates a 0.06% EQE and a brightness of 12 cd/m^2, which are 3 times less than pure PPV device. As previously discussed, this blend forms large scale ($>1\ \mu$m) patterns of PPV- and POX-rich phases. This morphology encompasses very little interfacial area between the electron and hole transporting domains, which obstructs the formation of excitons. Further, the very large POX domains may bridge between the electrodes, resulting in effective shorts in the device.

Current−voltage characteristics give further insight into the internal processes of the light-emitting diodes. In the self-assembled device, current pathways are extremely interrupted (perhaps due to the bimodal orientation of lamellae), resulting in reduced current densities as compared to the blend device in which the large domains of electron and hole transporting moieties lead to increased transport. (Figure 6) Interestingly, however, it is clear that the blend device is the least efficient and the least bright, indicating that this increased transport does not lead to increased recombination. It should be noted that none of the devices fabricated contained a specific layer tuned for emissive properties in order to simplify the study of self-assembly. This is an obvious route toward improved efficiencies. Further, eventual control of lamellar orientation will lead to greater insight into the charge and exciton dynamics within the device and is another route toward eventual efficiency improvement.

Conclusions

In conclusion, we demonstrate the synthesis of a new self-assembling rod−coil block copolymer containing electron and hole transporting blocks. The block copolymer self-assembles to form 15 nm lamellae oriented simultaneously both parallel and perpendicular to the substrate. The block copolymer shows much higher efficiencies and brightness than either pure PPV or an analogous PPV/POX blend. The thin film morphology of the block copolymer results in interruptions to charge transport and facilitates recombination. Consequently, the EQE and brightness of the self-assembled device are 2.7 times higher than the pure PPV device.

Acknowledgment. We gratefully acknowledge support from the Department of Energy Office of Basic Energy Sciences (DOE-BES) through the Plastic Electronics Program at Lawrence Berkeley National Laboratory (LBNL). Work at the Molecular Foundry was supported by the Office of Science, Office of Basic Energy Sciences, of the U.S. Department of Energy under Contract DE-AC02-05CH11231. SAXS experiments were performed at the Stanford Synchrotron Radiation Laboratory, a national user facility operated by Stanford University, and TEM experiments were performed at the National Center for Electron Microscopy at LBNL, both supported by the Department of Energy, Office of Basic Energy Sciences. GISAXS experiments were conducted at the Advanced Photon Source, supported by the U.S. Department of Energy, Office of Basic Energy Sciences, under Contract W-31-109-ENG-38. The authors thank the APS Sector 8 staff for assistance with these experiments and Bradley D. Olsen for helpful conversations regarding GISAXS analysis.

References and Notes

(1) Mitschke, U.; Bauerle, P. *J. Mater. Chem.* **2000**, *10* (7), 1471–1507.
(2) Shim, H. K.; Jin, J. I. *Polym. Photonics Appl. I* **2002**, *158*, 193–243.
(3) Chen, C. T. *Chem. Mater.* **2004**, *16* (23), 4389–4400.
(4) Veinot, J. G. C.; Marks, T. J. *Acc. Chem. Res.* **2005**, *38* (8), 632–643.
(5) Higgins, A. M.; Martin, S. J.; Thompson, R. L.; Chappell, J.; Voigt, M.; Lidzey, D. G.; Jones, R. A. L.; Geoghegan, M. *J. Phys.: Condens. Matter* **2005**, *17* (8), 1319–1328.
(6) Tang, C. W.; Vanslyke, S. A. *Appl. Phys. Lett.* **1987**, *51* (12), 913–915.
(7) Baldo, M. A.; O'Brien, D. F.; You, Y.; Shoustikov, A.; Sibley, S.; Thompson, M. E.; Forrest, S. R. *Nature (London)* **1998**, *395* (6698), 151–154.
(8) Baldo, M. A.; O'Brien, D. F.; Thompson, M. E.; Forrest, S. R. *Phys. Rev. B* **1999**, *60* (20), 14422–14428.
(9) Adachi, C.; Baldo, M. A.; Thompson, M. E.; Forrest, S. R. *J. Appl. Phys.* **2001**, *90* (10), 5048–5051.
(10) Sun, Y. R.; Giebink, N. C.; Kanno, H.; Ma, B. W.; Thompson, M. E.; Forrest, S. R. *Nature (London)* **2006**, *440* (7086), 908–912.
(11) Zhang, Y. D.; Hreha, R. D.; Jabbour, G. E.; Kippelen, B.; Peyghambarian, N.; Marder, S. R. *J. Mater. Chem.* **2002**, *12* (6), 1703–1708.
(12) Nuyken, O.; Bacher, E.; Braig, T.; Faber, R.; Mielke, F.; Rojahn, M.; Wiederhirn, V.; Meerholz, K.; Moller, D. *Des. Monomers Polym.* **2002**, *5* (2−3), 195–210.
(13) Muller, C. D.; Falcou, A.; Reckefuss, N.; Rojahn, M.; Wiederhirn, V.; Rudati, P.; Frohne, H.; Nuyken, O.; Becker, H.; Meerholz, K. *Nature (London)* **2003**, *421* (6925), 829–833.
(14) Ma, B.; Lauterwasser, F.; Deng, L.; Zonte, C. S.; Kim, B. J.; Frechet, J. M. J. *Chem. Mater.* **2007**, *19* (19), 4827–4832.
(15) Qiu, Y.; Duan, L.; Hu, X. M.; Zhang, D. Q.; Zheng, M.; Bai, F. L. *Synth. Met.* **2001**, *123* (1), 39–42.
(16) Lamansky, S.; Djurovich, P. I.; Abdel-Razzaq, F.; Garon, S.; Murphy, D. L.; Thompson, M. E. *J. Appl. Phys.* **2002**, *92* (3), 1570–1575.
(17) Bozano, L. D.; Carter, K. R.; Lee, V. Y.; Miller, R. D.; DiPietro, R.; Scott, J. C. *J. Appl. Phys.* **2003**, *94* (5), 3061–3068.
(18) Ahn, J. H.; Wang, C.; Pearson, C.; Bryce, M. R.; Petty, M. C. *Appl. Phys. Lett.* **2004**, *85* (7), 1283–1285.
(19) Lu, J. P.; Xia, P. F.; Lo, P. K.; Tao, Y.; Wong, M. S. *Chem. Mater.* **2006**, *18* (26), 6194–6203.
(20) Lee, Y. Z.; Chen, X. W.; Chen, S. A.; Wei, P. K.; Fann, W. S. *J. Am. Chem. Soc.* **2001**, *123* (10), 2296–2307.
(21) Tsolakis, P. K.; Kallitsis, J. K. *Chem.—Eur. J.* **2003**, *9* (4), 936–943.
(22) Jin, S. H.; Kim, M. Y.; Kim, J. Y.; Lee, K.; Gal, Y. S. *J. Am. Chem. Soc.* **2004**, *126* (8), 2474–2480.
(23) Furuta, P. T.; Deng, L.; Garon, S.; Thompson, M. E.; Frechet, J. M. J. *J. Am. Chem. Soc.* **2004**, *126* (47), 15388–15389.
(24) Lu, S.; Liu, T. X.; Ke, L.; Ma, D. G.; Chua, S. J.; Huang, W. *Macromolecules* **2005**, *38* (20), 8494–8502.
(25) Deng, L.; Furuta, P. T.; Garon, S.; Li, J.; Kavulak, D.; Thompson, M. E.; Frechet, J. M. J. *Chem. Mater.* **2006**, *18* (2), 386–395.
(26) Chen, P.; Yang, G. Z.; Liu, T. X.; Li, T. C.; Wang, M.; Huang, W. *Polym. Int.* **2006**, *55* (5), 473–490.
(27) Ma, B.; Kim, B. J.; Deng, L.; Poulsen, D. A.; Thompson, M. E.; Frechet, J. M. J. *Macromolecules* **2007**, *40* (23), 8156–8161.
(28) Bates, F. S.; Fredrickson, G. H. *Phys. Today* **1999**, *52* (2), 32–38.
(29) Semenov, A. N.; Vasilenko, S. V. *Zh. Eksp. Teor. Fiz.* **1986**, *90* (1), 124–140.
(30) Semenov, A. N. *Mol. Cryst. Liq. Cryst.* **1991**, *209*, 191–199.
(31) Halperin, A. *Europhys. Lett.* **1989**, *10* (6), 549–553.
(32) Halperin, A. *Macromolecules* **1990**, *23* (10), 2724–2731.
(33) Williams, D. R. M.; Fredrickson, G. H. *Macromolecules* **1992**, *25* (13), 3561–3568.
(34) Williams, D. R. M.; Halperin, A. *Phys. Rev. Lett.* **1993**, *71* (10), 1557–1560.
(35) Reenders, M.; ten Brinke, G. *Macromolecules* **2002**, *35* (8), 3266–3280.
(36) Pryamitsyn, V.; Ganesan, V. *J. Chem. Phys.* **2004**, *120* (12), 5824–5838.
(37) Chen, J. T.; Thomas, E. L.; Ober, C. K.; Mao, G. P. *Science* **1996**, *273* (5273), 343–346.
(38) Lee, M.; Cho, B. K.; Kim, H.; Yoon, J. Y.; Zin, W. C. *J. Am. Chem. Soc.* **1998**, *120* (36), 9168–9179.
(39) Ryu, J. H.; Oh, N. K.; Zin, W. C.; Lee, M. *J. Am. Chem. Soc.* **2004**, *126* (11), 3551–3558.
(40) Li, C. Y.; Tenneti, K. K.; Zhang, D.; Zhang, H. L.; Wan, X. H.; Chen, E. Q.; Zhou, Q. F.; Carlos, A. O.; Igos, S.; Hsiao, B. S. *Macromolecules* **2004**, *37* (8), 2854–2860.

(41) Tenneti, K. K.; Chen, X. F.; Li, C. Y.; Tu, Y. F.; Wan, X. H.; Zhou, Q. F.; Sics, I.; Hsiao, B. S. *J. Am. Chem. Soc.* **2005**, *127* (44), 15481–15490.
(42) Radzilowski, L. H.; Stupp, S. I. *Macromolecules* **1994**, *27* (26), 7747–7753.
(43) Radzilowski, L. H.; Carragher, B. O.; Stupp, S. I. *Macromolecules* **1997**, *30* (7), 2110–2119.
(44) Cho, B. K.; Chung, Y. W.; Lee, M. *Macromolecules* **2005**, *38* (24), 10261–10265.
(45) Sary, N.; Rubatat, L.; Brochon, C.; Hadziioannou, G.; Ruokolainen, J.; Mezzenga, R. *Macromolecules* **2007**, *40* (19), 6990–6997.
(46) Sary, N.; Brochon, C.; Hadziioannou, G.; Mezzenga, R. *Eur. Phys. J. E* **2007**, *24* (4), 379–384.
(47) Mao, G. P.; Wang, J. G.; Clingman, S. R.; Ober, C. K.; Chen, J. T.; Thomas, E. L. *Macromolecules* **1997**, *30* (9), 2556–2567.
(48) Jenekhe, S. A.; Chen, X. L. *Science* **1998**, *279* (5358), 1903–1907.
(49) Dai, C. A.; Yen, W. C.; Lee, Y. H.; Ho, C. C.; Su, W. F. *J. Am. Chem. Soc.* **2007**, *129* (36), 11036–11038.
(50) Lee, M.; Cho, B. K.; Kim, H.; Zin, W. C. *Angew. Chem., Int. Ed.* **1998**, *37* (5), 638–640.
(51) Lee, M.; Cho, B. K.; Kang, Y. S.; Zin, W. C. *Macromolecules* **1999**, *32* (22), 7688–7691.
(52) Gallot, B. *Prog. Polym. Sci.* **1996**, *21* (6), 1035–1088.
(53) Mao, G.; Ober, C. K. *Acta Polym.* **1997**, *48* (10), 405–422.
(54) Stupp, S. I. *Curr. Opin. Colloid Interface Sci.* **1998**, *3* (1), 20–26.
(55) Loos, K. M-G. S. *Supramolecular Polymers*; Ciferri, A., Ed.; Marcel Dekker: New York, 2000; pp 263−321.
(56) Lee, M.; Cho, B. K.; Zin, W. C. *Chem. Rev.* **2001**, *101* (12), 3869–3892.
(57) Olsen, B. D.; Segalman, R. A. *Mater. Sci. Eng. R* **2008**, *62* (2), 37–66.
(58) Olsen, B. D.; Segalman, R. A. *Macromolecules* **2005**, *38* (24), 10127–10137.
(59) Olsen, B. D.; Segalman, R. A. *Macromolecules* **2006**, *39* (20), 7078–7083.
(60) Olsen, B. D.; Segalman, R. A. *Macromolecules* **2007**, *40* (19), 6922–6929.
(61) Leclere, P.; Calderone, A.; Marsitzky, D.; Francke, V.; Geerts, Y.; Mullen, K.; Bredas, J. L.; Lazzaroni, R. *Adv. Mater.* **2000**, *12* (14), 1042–1046.
(62) Surin, M.; Marsitzky, D.; Grimsdale, A. C.; Mullen, K.; Lazzaroni, R.; Leclere, P. *Adv. Funct. Mater.* **2004**, *14* (7), 708–715.
(63) Chochos, C. L.; Tsolakis, P. K.; Gregoriou, V. G.; Kallitsis, J. K. *Macromolecules* **2004**, *37* (7), 2502–2510.
(64) Gunther, J.; Stupp, S. I. *Langmuir* **2001**, *17* (21), 6530–6539.
(65) Pereira, G. G.; Williams, D. R. M. *Macromolecules* **2000**, *33* (8), 3166–3172.
(66) Olsen, B. D.; Toney, M. F.; Segalman, R. A. *Langmuir* **2008**, *24* (5), 1604–1607.
(67) Olsen, B. D.; Li, X. F.; Wang, J.; Segalman, R. A. *Macromolecules* **2007**, *40* (9), 3287–3295.
(68) Moons, E. *J. Phys.: Condens. Matter* **2002**, *14* (47), 12235–12260.
(69) Milner, R. G.; Arias, A. C.; Stevenson, R.; Mackenzie, J. D.; Richards, D.; Friend, R. H.; Kang, D. J.; Blamire, M. *Mater. Sci. Technol.* **2002**, *18* (7), 759–762.
(70) Voigt, M.; Chappell, J.; Rowson, T.; Cadby, A.; Geoghegan, M.; Jones, R. A. L.; Lidzey, D. G. *Org. Electron.* **2005**, *6* (1), 35–45.
(71) Osaheni, J. A.; Jenekhe, S. A. *J. Am. Chem. Soc.* **1995**, *117* (28), 7389–7398.
(72) Becker, S.; Ego, C.; Grimsdale, A. C.; List, E. J. W.; Marsitzky, D.; Pogantsch, A.; Setayesh, S.; Leising, G.; Mullen, K. *Synth. Met.* **2001**, *125* (1), 73–80.
(73) Tzanetos, N. P.; Kallitsis, J. K. *Chem. Mater.* **2004**, *16* (13), 2648–2655.
(74) Chochos, C. L.; Kallitsis, J. K.; Gregoriou, V. G. *J. Phys. Chem. B* **2005**, *109* (18), 8755–8760.
(75) Stalmach, U.; de Boer, B.; Videlot, C.; van Hutten, P. F.; Hadziioannou, G. *J. Am. Chem. Soc.* **2000**, *122* (23), 5464–5472.
(76) de Boer, B.; Stalmach, U.; Melzer, C.; Hadziioannou, G. *Synth. Met.* **2001**, *121* (1−3), 1541–1542.
(77) Van De Wetering, K.; Brochon, C.; Ngov, C.; Hadziioannou, G. *Macromolecules* **2006**, *39* (13), 4289–4297.
(78) Sivula, K.; Ball, Z. T.; Watanabe, N.; Frechet, J. M. J. *Adv. Mater.* **2006**, *18* (2), 206–210.
(79) Hagberg, E. C.; Goodridge, B.; Ugurlu, O.; Chumbley, S.; Sheares, V. V. *Macromolecules* **2004**, *37* (10), 3642–3650.
(80) de Boer, B.; Stalmach, U.; van Hutten, P. F.; Melzer, C.; Krasnikov, V. V.; Hadziioannou, G. *Polymer* **2001**, *42* (21), 9097–9109.
(81) van der Veen, M. H.; de Boer, B.; Stalmach, U.; van de wetering, K. I.; Hadziioannou, G. *Macromolecules* **2004**, *37* (10), 3673–3684.
(82) Sivula, K.; Ball, Z. T.; Watanabe, N.; Frechet, J. M. J. *Adv. Mater.* **2006**, *18* (2), 206++.
(83) Ball, Z. T.; Sivula, K.; Frechet, J. M. J. *Macromolecules* **2006**, *39* (1), 70–72.
(84) Yang, X.; Loos, J. *Macromolecules* **2007**, *40* (5), 1353–1362.
(85) Scherf, U.; Gutacker, A.; Koenen, N. *Acc. Chem. Res.* **2008**, 000
(86) Kretzschmann, H.; Meier, H. *Tetrahedron Lett.* **1991**, *32* (38), 5059–5062.
(87) Yokoyama, A.; Yokozawa, T. *Macromolecules* **2007**, *40* (12), 4093–4101.
(88) Jeffries-El, M.; Sauve, G.; McCullough, R. D. *Macromolecules* **2005**, *38* (25), 10346–10352.
(89) Neef, C. J.; Ferraris, J. P. *Macromolecules* **2004**, *37* (7), 2671–2671.
(90) Benoit, D.; Chaplinski, V.; Braslau, R.; Hawker, C. J. *J. Am. Chem. Soc.* **1999**, *121* (16), 3904–3920.
(91) Lee, B.; Park, I.; Yoon, J.; Park, S.; Kim, J.; Kim, K. W.; Chang, T.; Ree, M. *Macromolecules* **2005**, *38* (10), 4311–4323.
(92) Tate, M. P.; Urade, V. N.; Kowalski, J. D.; Wei, T. C.; Hamilton, B. D.; Eggiman, B. W.; Hillhouse, H. W. *J. Phys. Chem. B* **2006**, *110* (20), 9882–9892.
(93) Opsteen, J. A.; van Hest, J. C. M. *Chem. Commun.* **2005**, (1), 57–59.
(94) Olsen, B. D.; Alcazar, D.; Krikorian, V.; Toney, M. F.; Thomas, E. L.; Segalman, R. A. *Macromolecules* **2008**, *41* (1), 58–66.
(95) Bates, F. S.; Rosedale, J. H.; Fredrickson, G. H. *J. Chem. Phys.* **1990**, *92* (10), 6255–6270.
(96) Eitouni, H. B.; Rappl, T. J.; Gomez, E. D.; Balsara, N. P.; Qi, S.; Chakraborty, A. K.; Frechet, J. M. J.; Pople, J. A. *Macromolecules* **2004**, *37* (23), 8487–8490.
(97) Sinha, S. K.; Sirota, E. B.; Garoff, S.; Stanley, H. B. *Phys. Rev. B* **1988**, *38* (4), 2297–2311.
(98) Segalman, R. A. *Mater. Sci. Eng. R* **2005**, *48* (3), 191–226.

MA800577G